Bioactive Materials 6 (2021) 2613–2628

Contents lists available at ScienceDirect

Bioactive Materials

journal homepage: www.sciencedirect.com/journal/bioactive-materials

Polydopamine-modified collagen sponge scaffold as a novel dermal regeneration template with sustained release of platelet-rich plasma to accelerate skin repair: A one-step strategy

Zijun Zheng [a,1], Minxiong Li [a,1], Pengwei Shi [b], Yanbin Gao [a], Jun Ma [a], Yuchen Li [a], Lei Huang [a], Zhangfeifan Yang [c], Lei Yang [a,*]

[a] Department of Burns, Nanfang Hospital, Southern Medical University, Jingxi Street, Baiyun District, Guangzhou, 510515, PR China
[b] Department of Emergency, Nanfang Hospital, Southern Medical University, Jingxi Street, Baiyun District, Guangzhou, 510515, PR China
[c] Department of Statistics, University of British Columbia, 2329 West Mall, Vancouver, V6T 1Z4, BC, Canada

ARTICLE INFO

Keywords:
Polydopamine
Sustained release
Platelet-rich plasma
Dermal regeneration template
Full-thickness skin defect

ABSTRACT

Although employed to release growth factors (GFs) for regenerative medicine, platelet-rich plasma (PRP) has been hindered by issues like burst effect. Based on collagen sponge scaffolds (CSSs) modified with polydopamine (pDA), a novel dermal regeneration template (DRT) was designed. However, whether it could efficiently deliver PRP and even foster wound healing remained unclear. In this work, after PRP was prepared and pDA-modified CSSs (pDA-CSSs) were fabricated, microscopic observation, GFs release assay and in-vitro biological evaluations of pDA-CSSs with PRP (pDA-CSS@PRP) were performed, followed by BALA-C/nu mice full-thickness skin defects implanted with pDA-CSS@PRP covered by grafted skins (termed as a One-step strategy). As a result, scanning electron microscope demonstrated more immobilized platelets on pDA-CSS′ surface with GFs' controlled release via enzyme-linked immunosorbent assay, compared with CSSs. In line with enhanced in-vitro proliferation, adhesion and migration of keratinocytes & endothelial cells, pDA-CSS@PRP were histologically revealed to accelerate wound healing with less scar via rapid angiogenesis, arrangement of more mature collagen, guiding cells to spread, etc. In conclusion, pDA-CSSs have potential to serve as a novel DRT capable of delivering PRP, which may foster full-thickness skin defect healing by means of a One-step strategy.

1. Introduction

As the largest organ of the body, the skin (consisted of epidermis, dermis and its appendices), acts as an important barrier against the invasion of foreign microorganisms, and has the functions of immunity, thermoregulation and metabolic activities [1]. Skin defects resulting from burns, chronic diseases, trauma, tumor resection, etc. often cause water-electrolyte imbalances and microbial invasion, threatening people's lives. Autografts, particularly split-thickness skin graft (STSG) or skin flap transplantation are considered to be important managements for aiding full-thickness skin defects [2,3]. Due to the disadvantages (e.g., complicated operation, severe damage to the donor area, bloated appearance, high failure rate, etc.), skin flap transplantation is not as widely used in clinical practice as skin grafts [4]. However, despite the better take-in in the early stage, skin grafts lacking sufficient dermal matrix, are often hindered by uncontrollable scar hyperplasia, lower mechanical resistance, etc. in the later phase, leading to graft failure or severe scar formation, which seriously affects the local appearance and functions [5]. How to avoid severe scar hyperplasia and contracture in the later phase is a key difficulty needing to be overcome in skin grafting.

Whether the skin graft has sufficient blood supply is the main factor affecting the quality of the skin graft [6]. Platelet-rich plasma (PRP) is a high-concentration platelet-oriented plasma obtained from animal or human whole blood via centrifugation [7], which typically 3- to 7-fold the mean platelet concentration in whole blood. Containing α-granules, platelets secrete several growth factors (GFs) after being activated, such as transforming growth factor-β (TGF-β), platelet-derived growth

Peer review under responsibility of KeAi Communications Co., Ltd.
* Corresponding author.
E-mail address: yuanyang@fimmu.com (L. Yang).
[1] These authors contributed equally to this work.

https://doi.org/10.1016/j.bioactmat.2021.01.037
Received 5 December 2020; Received in revised form 20 January 2021; Accepted 29 January 2021

factor (PDGF), vascular endothelial growth factor (VEGF), etc [8,9]. These GFs and other proteins (such as adhesion molecules and chemokines) interact with the local environment to promote cell differentiation and proliferation, which are responsible for re-epithelization and angiogenesis via mesenchymal cell recruitment and extracellular matrix synthesis [8,10]. Nevertheless, PRP is limited due to burst release and its short half-life, i.e., 95% of these GFs are secreted within an hour, quickly dilute and decay into the tissue fluid [11,12]. In this case, although secreted GFs promote angiogenesis and fibroblast maturation, this release process will inevitably cause numerous wastes of GFs. In practice, how to avoid the burst release and reduce the waste is a hot issue that needs to be addressed during the use process.

In the past decades, numerous bi-layer dermal substitutes have been developed and applied for the management of full-thickness skin defects, such as Alloderm® [13,14], Integra® [15,16], Pelnac® [17] and Lando®, of which the low-layer porous collagen sponge scaffold (CSS) function as dermal regenerate template (DRT). Being the main protein of the extracellular matrix, collagen has excellent biocompatibility low immunogenicity [18]. Moreover, collagen scaffold has attracted the most attention due to the sustained drug release properties [19]. The previous studies have demonstrated that the CSS have surface that can be functionalized, of high porous structure to provide a biomimetic three-dimensional microenvironment, possessing the ability to host drug molecules to sustain drug release [20]. On the other hand, the porous structure guide inward proliferation and migration of fibroblasts and endothelial cells, which promotes granulation tissue and angiogenesis for wound healing with less scar [21,22]. However, the second-step skin graft surgery is usually performed two to three weeks after CSS implantation [23], which increases the patients' pain and prolongs the patients' hospital stay. One-step skin grafting requires the dermal substitute and a STSG to be covered on the wound at the same time. The existence of non-vascular active dermal substitute may hinder the survival of the graft [24].

It is known that functional surface coatings mediate the cell−surface interaction between tissues and biomaterials, which provided alternative strategies for the improvement of bioactivities [25,26]. Polydopamine (pDA) inspired by mussels has biocompatibility with low cytotoxicity and improves the adhesion properties of biomaterials modified [27]. Under alkaline ambient conditions, dopamine (DA) dispersed in moisture and oxygen is susceptible to self-polymerize into pDA through covalent bonding, hydrogen bonding, π−π interactions, etc [28,29]. The functional groups of pDA such as amine, imine and catechol functionalities enable pDA to be a highly reactive substance which can adhere to a variety of materials' surface, including metals, hydrogel, ceramics, polymers and even Teflon [30,31]. Numerous previous studies have demonstrated pDA to have surface immobilization of biologically active molecules. For instance, after synthesizing PDA-coated gold NPs, Liu et al. [32] investigated their biocompatibility and stability in vivo. And Chen et al. [33]. applied pDA in three-dimensional (3D) printing technology to fabricate porous degradable bone repair scaffolds. In particular, pDA has great potential as surface coating strategy to avoid initial burst effect onto various drug delivery matrices [34–36].

Herein, we hypothesized that CSSs coated with pDA (pDA-CSSs) might display improved outcomes for skin wound healing. To confirm this, pDA-CSSs were fabricated and subsequently characterized via micromorphology and in vitro biological evaluations. Furthermore, a nude mouse model with full-thickness skin defects was established, and pDA-CSSs delivering PRP was applied to repair the defects with a full-thickness skin graft (as a One-step surgical procedure). This novel scaffold's DRT function and drug delivery efficiency in vivo would be further evaluated.

2. Materials and methods

2.1. Fabrication of CSSs

Unlike the bilayer artificial dermis commercially available, the CSSs were a single-layer structure (without a silicone layer) consisted of collagen and polysaccharides, which were fabricated as reported previously [37]. Briefly, type I collagen derived from bovine tendon was selected in the whole process, and a collagen solution was prepared with the addition of a mass fraction of 0.6% chondroitin sulfate. After being poured into special molds and dried by a freeze dryer, the mixture was then subjected to thermal cross-linking at 105 °C under vacuum, followed by another freeze-dry to obtain the desired CSSs. Micromorphology observation was conducted via Scanning Electron Microscope (SEM; TM3030, HITACHI).

2.2. Fabrication of pDA-CSSs

After dopamine hydrochloride (2 mg/mL) was dissolved in 10 mM Tris-HCl (pH 8.5), hydrated CSSs were immersed in the oxygen-containing solution to be modified in a horizontal rotation mode (50 rpm, 12 h) at room temperature [38]. Next, the pDA-coated samples were ultrasonically rinsed with deionized water 10 times (for 5 min each time), and clean pDA-CSSs sterilized by irradiation were air tightly stored in phosphate-buffered saline (PBS). SEM (MIRA3, TESCAN; TM3030, HITACHI) and Atomic Force Microscope (AFM; Dimension ICON, BRUKER) were employed to observe the microstructure with unmodified CSSs as a control.

2.3. Isolation of PRP from Bama miniature pig

All procedures were in line with the Institutional Animal Care and Use Committee (IACUC) and were approved by the Animal Experimentation Ethics Committee of Nanfang Hospital. One male Bama miniature pig (weighing ~ 40 kg) was anesthetized with isoflurane (Sevorane®; Abbott AG, Baar, Switzerland) in oxygen applied by the facemask. Skin patch was shaved, washed with sterile physiological saline, wiped dry with sterile gauze and disinfected with iodophor [39]. A total of ~180 mL of whole blood was collected from the jugular vein and quickly dispensed into a test tube containing 1 mL of sodium citrate (10% volume fraction) as an anticoagulant. After the blood was firstly centrifuged at 300 g for 10 min as previously reported [40,41], the upper layer (platelet-poor plasma, PPP) and the middle buffy-layer (containing platelets & leukocytes) were together pipetted out into another tube for further centrifugation (1000 g, 10 min). The bottom layer in white was suspended with modest PPP to obtain PRP, temporarily stored at 4 °C.

2.4. PRP adhesion and characterization of immobilization efficiency of platelets

In order to enable PRP fully contact with the scaffolds, the adhesion process was carried out by uniformly rotating and mixing. Briefly, the pDA-CSS were immersed into PRP and mixed in a horizontal rotation mode (50 rpm, 12 h) at room temperature (like the modification of pDA-CSSs above). These scaffolds were then rinsed twice with PBS to remove unattached platelets. To characterize the immobilization efficiency of platelets, the pDA-CSSs were also fixed in 2.5% glutaraldehyde for 2 h, followed by being rinsed again with deionized water three times. Then the samples were dehydrated in ethanol in a medium gradient: 50%, 70%, 80%, 90%, 100%, 100%, each gradient was 15min. The dehydrated samples were then transferred in a refrigerator at −86 °C and underwent lyophilization in a freeze dryer for 12 h. After each sample was fixed on an aluminum sample platform and sputter-coated with a thin layer of gold under vacuum via a sputtering machine (JS-17085, KYKY), SEM (HITACHI TM3030) was employed to observe platelets

immobilized on pDA-CSSs' surface with CSSs (unmodified) as a control.

2.5. In vitro GFs release assay

Enzyme-linked immunosorbent assay (ELISA) was applied to quantify the GFs' release profiles, such as that of VEGF (n = 5) and PDGF-BB (n = 5). By means of the adhesion of PRP introduced above, the pDA-CSS with PRP (pDA-CSS@PRP) was prepared. Rapidly, the release of the VEGF and PDGF-BB from the pDA-CSS@PRP (immersed in 500 μL PBS) at 6, 12, 24, 48, 72, and 96 h after the activation with 4% $CaCl_2$ (at a ratio of 7:1 to the buffer, 37 °C) was evaluated using VEGF and ELISA kits (R&D Systems, USA). Single PRP and CSSs with PRP attached (CSS@PRP) served as controls.

2.6. In vitro cell viability

2.6.1. Cell proliferation and adhesion

HUVECs and HaCaT cells were respectively seeded on each group of scaffolds in a 96-well plate at a density of 10^5 cells/mL, and cultured at 37 °C for 7 days, with medium exchange culture every 1–2 days. On day 7 of culture, the samples were taken out of the incubator, underwent two washes with PBS and 20-min fixation with 4% paraformaldehyde at room temperature. After the fixative was washed off with PBS, the cells were sequentially penetrated with 0.1% Triton X-100 (REF# V900502, Sigma) and blocked with 1% bovine serum albumin (BSA; REF# V900933, Sigma). Subsequently, 5 μg rhodamine-labeled phalloidin (P1951, Sigma) and the 4', 6-diamidino-2-phenylindole (DAPI; REF# D9542, Sigma) solution were utilized to stain the cytoskeletons and the cell nuclei in a dark room, respectively. Finally, a laser scanning confocal microscopy (LSCM; SP8, Leica) was used to obtain images of cell proliferation and adhesion at 405/552 nm, with five fields being recorded each sample.

2.6.2. Scratch wound assay

For the scratch wound assay, HaCaT cells and HUVECs were plated into 6-well plates at 5×10^5 cells/well (3 replicates per group) and incubated until the confluence in a 37 °C incubator. Then the pipette tip was used to make a scratch on the cell layer at a constant speed on the back of the plate. After 3 washes with PBS, 24-mm inserts (3 μm pore polyester membrane, REF# 3492, Corning) were placed into 6-well plates (REF# 3492, Corning), and pDA-CSS@PRP, CSS@PRP, CSS were transferred onto the inserts. Subsequently, serum-free medium was added to the plates until the scaffolds could be totally immersed. The cell migration of each group was photographed and recorded at 0 h, 6 h, 12 h, 24 h, 48 h. Cell migration area was calculated using the following formula: Migration Rate (MR) (%) = $(R_0 - R_n)/R_0 \times 100\%$, of which R_0 represents the area of initial scratch area, R_n represents the remaining unclosed scratch area.

2.7. In vivo wound healing in a full-thickness skin model

In keeping with the ethical standards of the IACUC, this study was approved by the Animal Experimentation Ethics Committee of Nanfang Hospital, Southern Medical School, China. Efforts were made to minimize animal suffering and the number of rodents utilized in this study. Male BALA-C/nu mice (n = 30, weighting 20–24 g) were purchased from the Experimental Animal Center of Southern Medical University. And these animals with free access to standard food and water were maintained in a specific pathogen-free environment (22 ± 2 °C) with a 12-h light/dark cycle.

After one-week adaptation to the environment before the launch of experiment, the animals were randomly divided into four groups based on the different grafts employed to the wound bed: pDA-CSS@PRP, CSS@PRP, CSS and Normal Saline (NS, as a blank control). Above all, these mice were placed in an induction chamber with isoflurane (3% in O_2 at 0.6 L/min) to induce anesthesia. Then, the mouse was immediately transferred onto a heating pad (at 38 °C setting) in a prone position with the limbs stretched. Meanwhile, the gas flow was reduced to 0.3 L/min for maintenance of general anesthesia with a nose cone. Two round full-thickness excisional wounds with a diameter of 12 mm were created on the dorsum with iris scissors under sterile surgical conditions. By removing the deep partial dermis and panniculus carnosus away, the excised skins were trimmed into full-thickness skin grafts, stored in saline gauze for later use. In order to compare different groups on the same individual, various interventions were cross-paired and implanted into two wound beds, covered by full-thickness skin graft with intermittent suture. Silicone rings were fixed around the wound to prevent wound contraction (Scheme 1). One Vaseline gauze, gauze ball and sterile dressing (REF# 1624w, 3 M Healthcare)were applied on top of the skin grafts in sequence to provide appropriate pressure and prevent scratching, with external dressings replaced every other day.

2.8. Survival, contraction and capillary density of skin grafts

On postoperative day 3, 5, 7, 14 and 21, six mice (a total of twelve wounds, each group in triplicate) were randomly sacrificed by carbon dioxide inhalation. The wound sites were photographed with a digital camera and quantified using Image J software (version 1.50i). The skin graft survival was expressed by using the following formula: Wound healing rate = [1- (Unhealed skin graft size/Traced area size)] × 100%. On day 21, the margin of each grafted skin was also carefully traced to assess the skin graft contraction, which was calculated as followed: Wound shrinkage rate = [1- (Traced area size/Original wound size)] × 100%.

With the purpose of morphologically recording the generated blood vessels, the grafts and surrounding tissues were harvested to be flattened on a transparent petri dish. A white light source is set from the bottom of the petri dish to illuminate the samples, so that the blood vessels were easily visible, which were photographed and recorded. All samples were then fixed in 4% paraformaldehyde at 4 °C, followed by dehydration through series of ethanol wash, and then embedded in paraffin.

2.9. H&E and Masson's trichrome staining

Paraffin-embedded samples which were cut into slices with 4 μm thickness in cross-section were utilized for histological staining. After dewaxation and rehydration, Hematoxylin and eosin (H&E) staining and Masson's trichrome staining were conducted to histologically measure the number of new blood vessels, thickness of the granulation tissue and the deposition of collagen following the manufacturer's (Sigma). Images were taken via an automatic section scanner (C10730-12, HAMAMATSU). Vascularization of samples was evaluated by counting the capillaries in 5 fields of each H&E section, performed by two blinded reviewers. Thickness of the granulation tissue and collagen density & deposition were measured by analyzing images using ImageJ as described previously [42].

2.10. Immunohistochemistry of CD31 and Ki67

To further evaluate angiogenesis and cell proliferation in wound tissue, immunohistochemistry of CD31 and Ki67 were employed, respectively, of which the treatments were carried out in accordance with the established method [43,44]. Briefly, after undergoing these processes such as deparaffinization, rehydration and antigen retrieval, sections were incubated by Hydrogen peroxide block and Protein block in turns. Immunohistochemical staining was performed using primary antibodies against CD31(1:25; REF# ab28364, Abcam) and Ki67 (1:2000; REF# ab15580, Abcam) at 4 °C overnight, followed by secondary antibody. Angiogenesis and cell proliferation were evaluated by counting the number of brown-labeled vessel-like structures and brown-labeled nuclei, respectively. Images were acquired with an automatic section scanner from five fields of each section and the

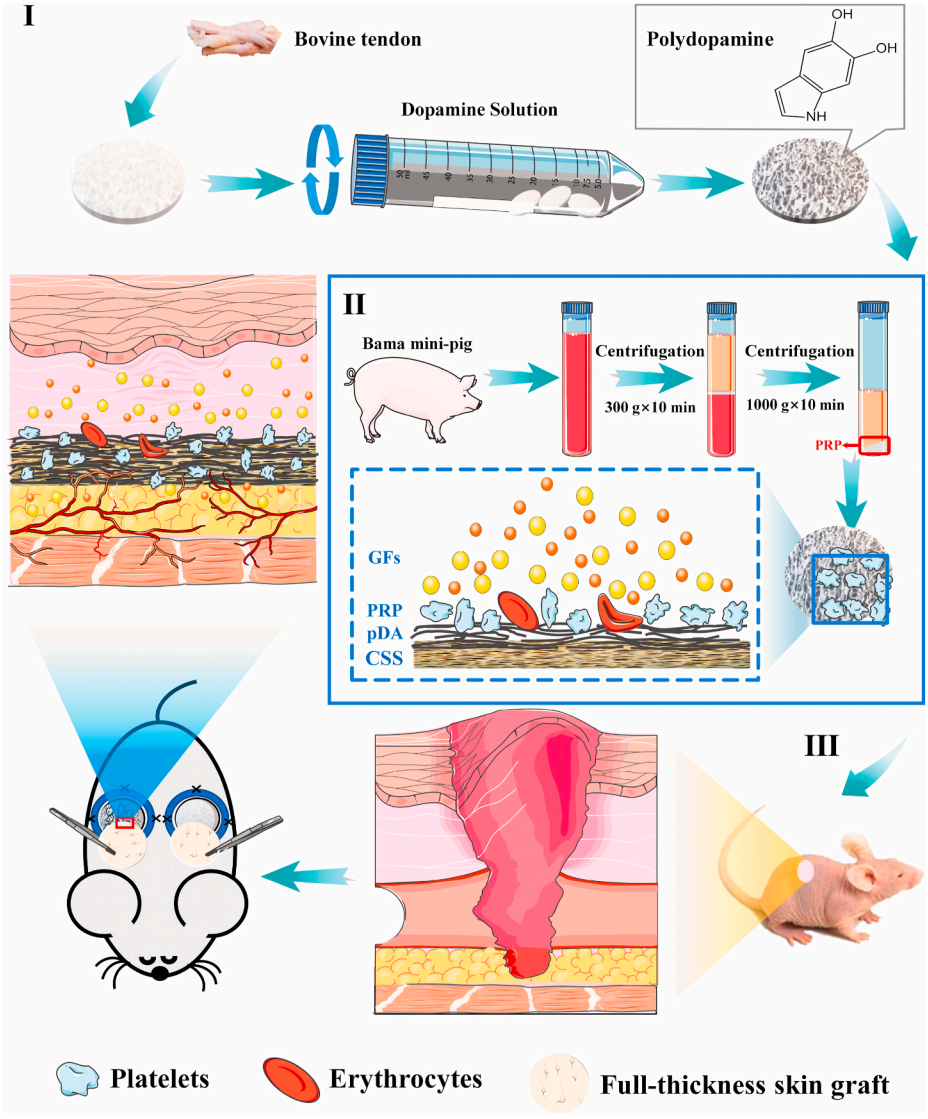

Scheme 1. Schematic overview of the preparation of polydopamine-modified collagen sponge scaffold with platelet-rich plasma (pDA-CSS@PRP) and bio-application. (I) The preparation of CSS. (II) The CSS is combined with PRP promoting the release of GFs. (III) The pDA-CSS@PRP and STSG transplanted by One-step to accelerate full-thickness skin defect wound healing.

quantification were performed using ImageJ software.

2.11. Statistical analysis

All quantitative data were recorded with SPSS software (version 23.0, IBM Corporation) and presented as mean ± standard deviation. Statistical comparisons between groups were performed using Independent Student's t-test or one-way ANOVA when appropriate. Values of $P < 0.05$ (*) and $P < 0.01$ (**) were considered statistically significant, and *ns* indicated not significant.

3. Results

3.1. Characterization of pDA-CSS

In this experiment, CSSs are different from the artificial dermis commercially available in that they are a single layer scaffold mainly composed of collagen I extracted from bovine tendon. After being prepared, the scaffolds were transferred to dopamine solution to allow the spontaneous oxidative polymerization of dopamine to form the pDA-CSSs.

The SEM images at low magnification (Fig. 1I) manifested that these pDA-coated CSSs retained a porous network structure like CSSs without modification, meaning the original structure was not destroyed upon the introduction of pDA. Allow for the surface morphology and roughness of materials play an important role in changing the cell-scaffold interaction [45], the three-dimensional microstructure of pDA-CSSs and CSSs were further observed by SEM at high magnification and AFM. In line with the SEM at high magnification (Fig. 1, II & III), AFM revealed the micro-morphology of unmodified CSS was homogenous and slightly rough whereas the roughness considerably increased for the pDA-CSS in which, moreover, the presence of randomly distributed self-polymerize particles could be clearly observed.

3.2. Microscopic observation of PRP immobilized on pDA-CSSs

The whole blood was separated by a two-step centrifugal separation method to prepare PRP, and the concentrated platelets were immobilized on the surface of pDA-CSS. Compared with unmodified CSSs, SEM images (Fig. 2I) demonstrated more PRP (or platelets) were immobilized onto the pDA-CSSs, which means pDA modification could significantly increase the loading of PRP (or platelets) on the biomaterial.

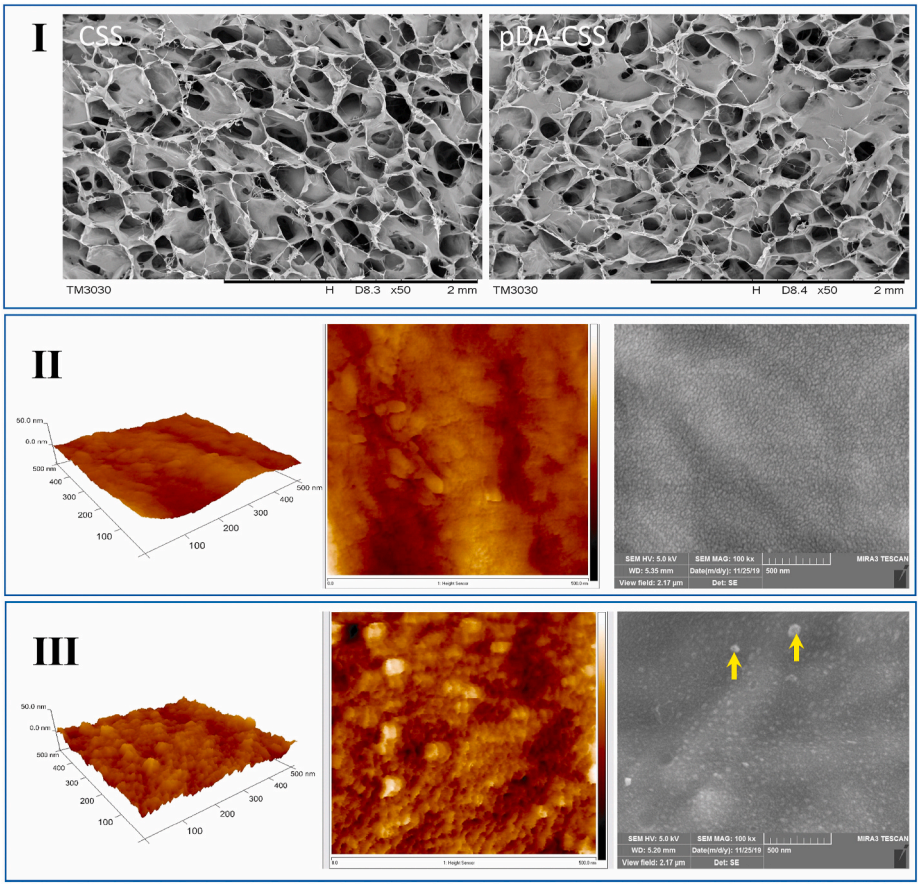

Fig. 1. Microstructure of pDA-CSS and CSS. (I) SEM images of CSS and pDA-CSS at low magnification. (II) Ultrastructure characteristics of CSS by AFM and SEM. (III) Ultrastructure characteristics of pDA-CSS by AFM and SEM. The self-assembled pDA was pointed by a yellow arrow. (For interpretation of the references to color in this figure legend, the reader is referred to the Web version of this article.)

Interestingly, some platelets attached to the pDA-CSS were seen to be activated, which was attributed to the tight connection to CSS and the further interaction with collagen, as previously reported [46].

3.3. Growth factors release detection

The release of VEGF and PDGF-BB from the PRP, CSS@PRP, and pDA-CSS@PRP groups were evaluated with ELISA. The PRP group had an immediate release of VEGF and PDGF-BB in the first 6 h after which the release decreased rapidly, no subsequent release after 72 h for VEGF and after 48 h for PDGF-BB. In contrast, the pDA-CSS@PRP group released a relatively high amount of both GFs and showed a prolonged release ($P < 0.05$). Following incubation for 96 h, the VEGF still maintained at 34.5% of its peak in the pDA-CSS@PRP group, and 5.6% of its peak in the CSS@PRP group. In line with that of VEGF, the release of PDGF-BB in pDA-CSS@PRP group displayed the same trend ($P < 0.05$), and a maintained release of 7.7% of its peak was found until 96 h.

3.4. In vitro cytological evaluation

3.4.1. Cell adhesion and proliferation

In order to prove the effect of these different scaffolds on cell adhesion and proliferation, the cytoskeleton was stained with Alexa Fluor 564 Phalloidin, and the nucleus was stained with DAPI for immunofluorescence observation [22]. As showed in Fig. 3I, the seeded cells adhered firmly to the scaffolds in each group on day 7, a typical cobblestone morphology was clearly observed to represent HaCaT cells and a polygonal morphology to represent HUVECs. In addition, more cells had fully spread inside the pores of pDA-CSS@PRP and closely packed together, which indicated that better promotion of cell adhesion and proliferation were achieved than unmodified CSSs with or without PRP ($P < 0.05$).

3.4.2. Cell migration

In-vitro cell migration was evaluated based on HUVECs and HaCaT cells and the results are displayed in Fig. 4. At 24 h after scratching, HaCaT cells cultured in the presence of pDA-CSS@PRP exhibited a significantly increasing migration rate (Fig. 4II, $P < 0.05$), and the cells on both sides have contacted each other. At 48 h, the gap between HaCaT cells of CSS@PRP was also closed (Fig. 4I). The migration rate of HUVECs in the pDA-CSS@PRP, CSS@PRP and CSS groups at 6 h was 36.7 ± 0.47%, 26.91 ± 0.24% and 15.44 ± 0.35%, respectively, which was statistically significant (Fig. 4IV, $P < 0.05$). The HUVECs intercellular space was closed after 24 h in the pDA-CSS@PRP group, while that in the CSS@PRP group was closed after 48 h (Fig. 4III). The result demonstrated that pDA-CSS@PRP indeed played an important role in improving the migration of both HUVECs and HaCaT cells.

3.5. In vivo wound healing in a full-thickness skin model

In order to further evaluate the application of wound healing, full-thickness dorsal wounds were performed to confirm the positive effects of pDA-CSSs with PRP adhered as a wound dressing in vivo. We choose to transplant two different scaffolds on the same mouse and use the same breeding conditions to exclude the influence of individual and external factors on the experimental results (Fig. 5I).

In Fig. 5 (II-IV), the repaired skin was clearly distinguished from the surrounding normal skin because of the suture knots. After 5 days of

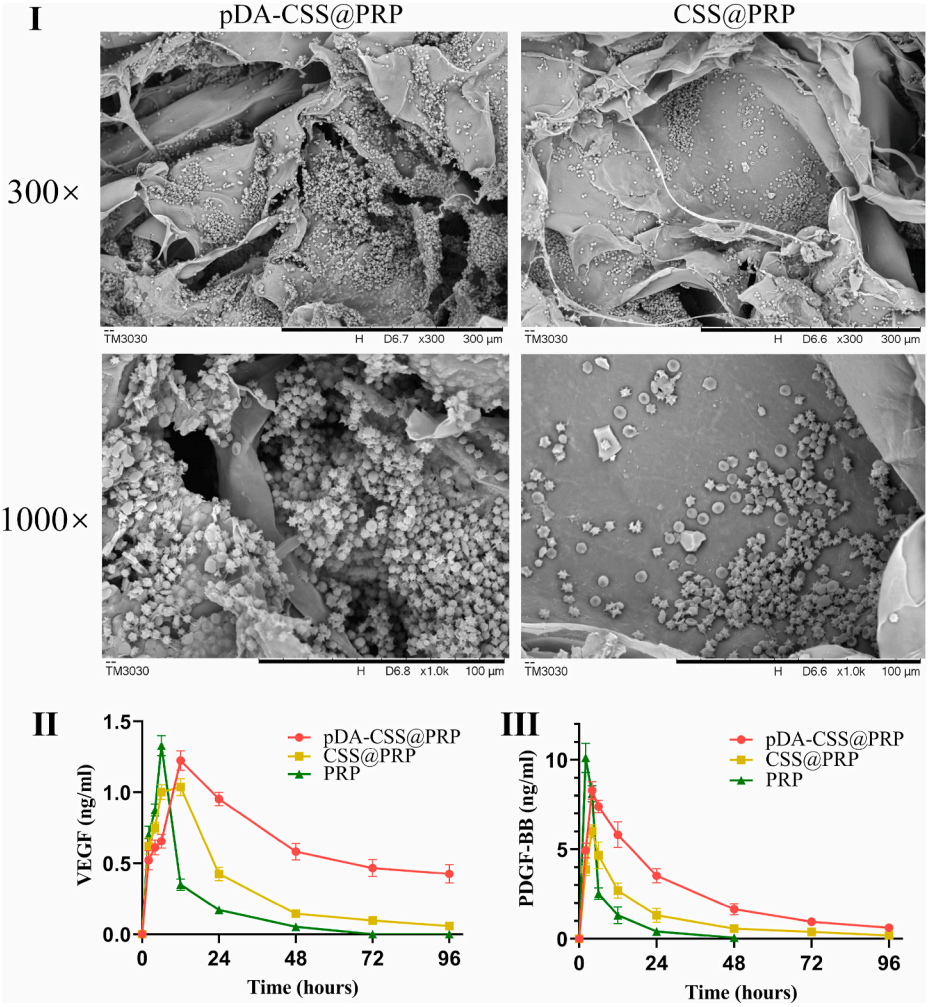

Fig. 2. Characterization of pDA-CSS@PRP. (I) SEM of pDA-CSS@PRP and CSS@PRP. (II) Release profiles of VEGF. (III) Release profiles of PDGF-BB.

treatment, the skin survival rate of pDA-CSS@PRP, CSS@PRP, CSS and blank control were 41.01 ± 2.81%, 33.10 ± 2.82%, 26.18 ± 5.02% and 29.57 ± 0.49%, which showed a significant increase of early survival in the pDA-CSS@PRP group ($P < 0.05$). On day 7 and 14, it was observed that the full-thickness skin graft in the pDA-CSS@PRP group appeared a pink and dry surface with an indistinctive wound edge, while that of CSS exhibited a more exudate appearance. Quantification of the skin survival rate indicated significantly rapid healing rate of the pDA-CSS@PRP treatment ($P < 0.01$). Finally, on day 21, the wounds in pDA-CSS@PRP and CSS@PRP groups were almost completely healed (95.84 ± 1.90% and 84.53 ± 3.69%), displaying a morphological appearance closer to the original uninjured tissue, which suggested that PRP could enhance the cutaneous wound healing, and pDA modification furtherly enlarged this therapeutic effect ($P < 0.01$). Notably, though without statistical significance, the wound shrinkage rate in the blank control group (19.72 ± 3.84%) was more higher than that in the three scaffold groups (14.63 ± 2.93 for pDA-C@PRP, 14.63 ± 3.39% for CSS@PRP and 16.94 ± 3.13% for CSS) after 21 days of treatment (Fig. 6), which might be attached great importance to the DRT as previously reported [2].

3.6. Histology analyses

3.6.1. Cellularity and vascularization via H&E staining

To further distinguish the ultimate survival's quality of full-thickness skin grafts in each group, the tissue specimens were harvested for the histological analysis via H&E staining on day 21. Fig. 7I showed a whole morphology with enlarged cross-sectional images of skin grafts and scaffolds. According to the whole morphology, the full-thickness skin grafts in each group all survived well on day 21, and no obvious gap was observed between the skin graft and the regenerative tissue. In pDA-CSS@PRP and CSS@PRP groups, new blood vessels and fibrous structure were distributed almost along the edge of the scaffolds, with little obvious necrotic tissue occurring, while plenty of inflammatory cells had infiltrated into the graft's dermis in the CSS group and surrounded the degenerated or coagulated necrotic hair follicles.

As presented in Fig. 7II, the thickness of newly formed granulation tissue in pDA-CSS@PRP (98.65 ± 34.35 μm) was thicker than that in CSS@PRP (61.88 ± 14.91 μm), CSS (44.69 ± 13.57 μm) and black control group (25.58 ± 6.57 μm) ($P < 0.05$). And the quantification of new blood vessels in the pDA-CSS@PRP group was also significantly demonstrated higher than the other three groups (Fig. 7III, $P < 0.05$). In skin graft layer, more neovascularization was further noticed in the pDA-CSS@PRP group with less inflammatory cell infiltration and necrotic tissue, distinguished from the CSS. In addition, it was seen from the magnified view of the scaffold layer that more fibroblasts and extracellular matrix proliferated and infiltrated into pDA-CSS delivering PRP with desired neovascularization, instead of successively decreasing spreading cells in CSS@PRP and CSS in turns.

3.6.2. Collagen deposition and maturation via Masson's trichrome staining

Masson's trichrome staining and analysis were used to describe the collagen deposition and maturation in wounds. As displayed in Fig. 8, aniline blue dye was utilized to labeled collagen (in blue), whose

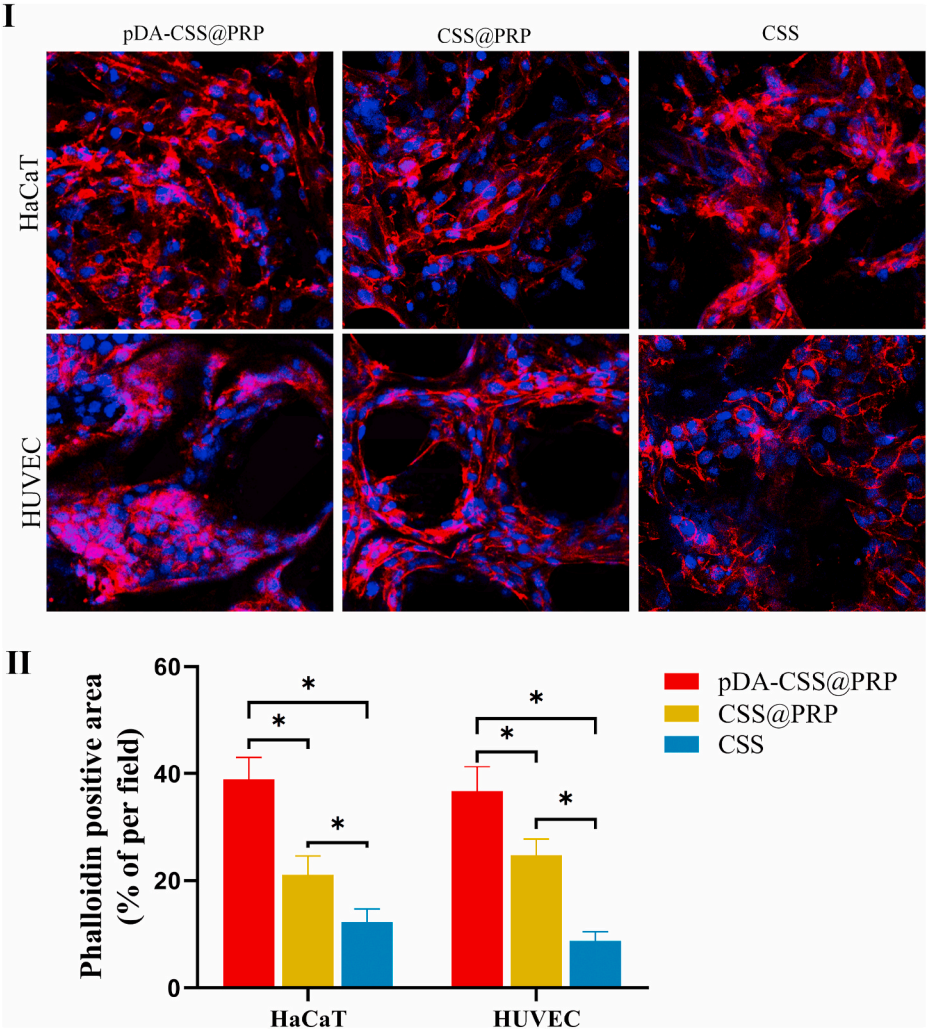

Fig. 3. Cell adhesion and proliferation in vitro. (I) Immunofluorescence staining of HaCaT and HUVEC in different groups. (II) Quantitative statistics of fluorescence intensity per field (*$P < 0.05$).

maturity and accumulation were positively correlate with and the degree of color. And notable histological observations are highlighted at high magnification (Fig. 8II). To be brief, dense and thick collagen in the pDA-CSS@PRP group was easily observed with a deeper blue color and the regular arrangement, while some blank areas conversely remained without collagen filling in other groups, especially in the blank control group, which was verified in statistical data of the collagen index (CI; the intensity of collagen fibers accumulation [42], Fig. 8III). Obviously, the pDA-CSS@PRP group exhibited increasing mature collagen with well-organized deposition compared to other groups, while the disorderly immature state of collagen in blank control group might contribute to scar hyperplasia and shrinkage.

3.7. Immunohistochemistry

3.7.1. Angiogenesis

Angiogenesis plays a vital role in the entire wound healing process because blood vessels provide progenitor cells, oxygen and nutrients to maintain the proliferation and remodeling of cell tissues. Vascular endothelial cells were marked by CD31 to confirm the degree of tissue neovascularization [6]. On postoperative day 21, the pDA-CSS@PRP group displayed greater amounts of new blood vessels with stronger branches under the full-thickness skin graft (Fig. 9, I & II). For further histological evaluation, CD31 immunohistochemistry staining demonstrated the pDA-CSS@PRP group possessed increasing neovascularization [50 ± 8/(high power field, HPF)] compared with the CSS@PRP group (36 ± 4/HPF), CSS group (16 ± 4/HPF) and blank control group (27 ± 6/HPF) (Fig. 9III, $P < 0.05$).

3.8. Cell proliferation

Ki67 is a nuclear antigen expressed in proliferating cells, which makes cells in the proliferation cycle appearing brown [47]. In the process of wound healing, various types of cells are involved at different stages, including keratinocytes, endothelial cells, fibroblasts, inflammatory cells, etc. [48], which were labeled by immunohistochemistry staining for Ki67 in this experiment. As illustrated in Fig. 10I, the layer of full-thickness skin grafts (blue box) and scaffold edge (red box) were selected for partial magnification observation. In accordance with the edge of the scaffolds, more proliferating cells in the skin grafts were demonstrated in the pDA-CSS@PRP group than others. Quantitatively, cell proliferation was the most active in the pDA-CSS@PRP (172 ± 45/HPF), followed by CSS@PRP (68 ± 16/HPF), blank control (18 ± 8/HPF) and CSS (34 ± 12/HPF), which was statistically significant (Fig. 10II, $P < 0.05$). What's more, another significant increase of Ki67 positive cells were also observed in the scaffold of pDA-CSS@PRP (Fig. 10III, $P < 0.05$), which implied its better promotion for skin repair related cells' adhesion and proliferation, in keeping with in-vitro cytological evaluation above.

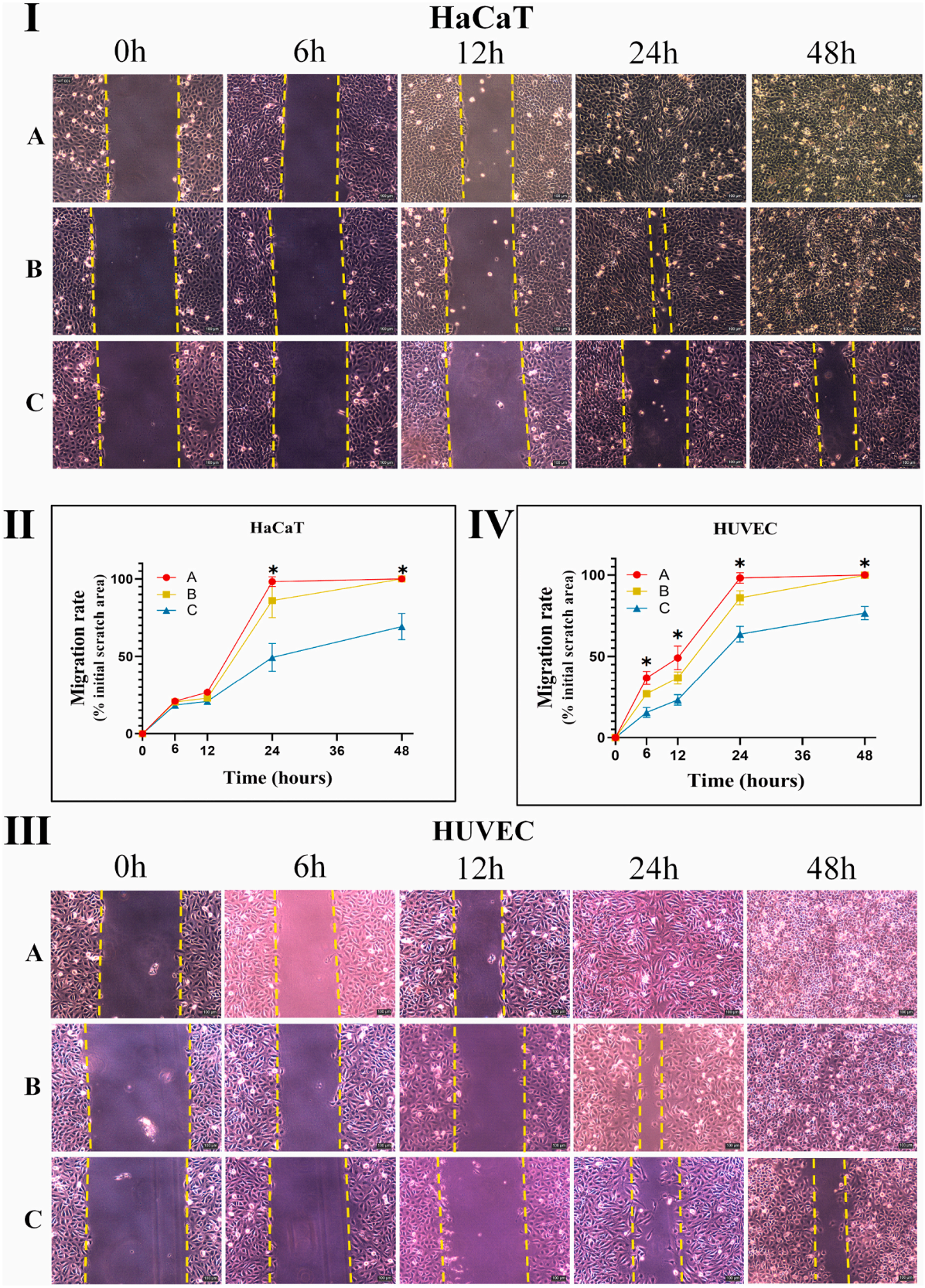

Fig. 4. Scratch assay to detect the migration of HaCaT cells and HUVECs. (I) The migration state of HaCaT. A, B and C indicate pDA-CSS@PRP, CSS@PRP and CSS, respectively. (II) Quantification of HaCaT migration rate. (III) The migration state of HUVEC. (IV) Quantification of HUVEC migration rate (*$P < 0.05$).

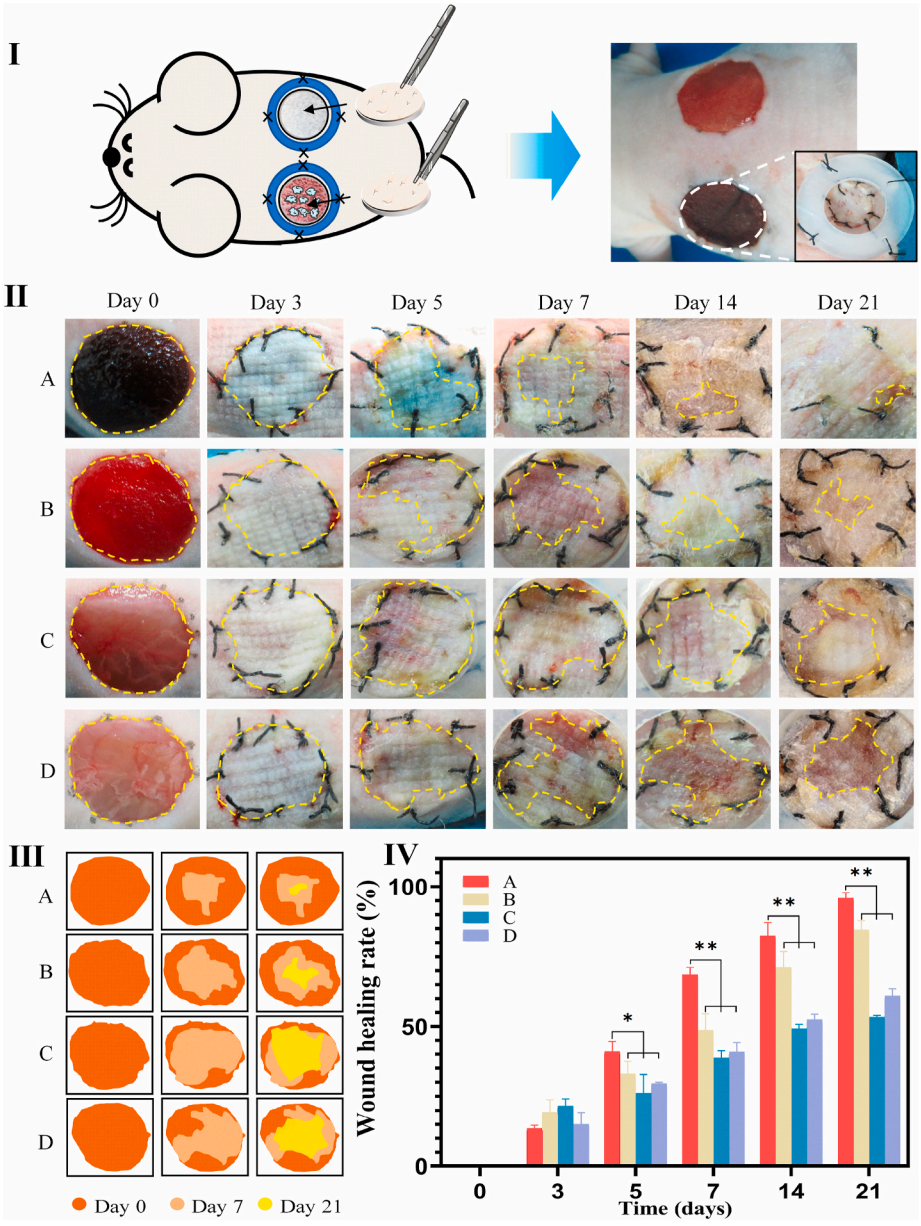

Fig. 5. Macroscopic wound healing evaluation. (I) Schematic diagram of the application of different scaffolds in mouse wounds. (II) Representative images of survival status of full-thickness skin grafts at each time point post wounding. A, B, C and D indicate pDA-CSS@PRP, CSS@PRP, CSS and blank control, respectively. The edges of unhealed wounds were circled in yellow dotted lines. (III) Schematic diagram of unhealed wound edges of the four groups on day 0, 7 and 21 post wounding. (IV) Quantification of wound healing rate (*$P < 0.05$, **$P < 0.01$). (For interpretation of the references to color in this figure legend, the reader is referred to the Web version of this article.)

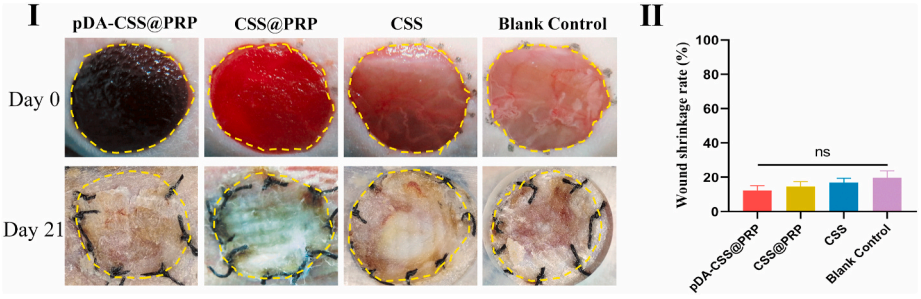

Fig. 6. Wound shrinkage of mice on days 21 post-operation. (I) Macroscopic images of wound shrinkage in different groups. (II) Quantitative statistics of wound shrinkage rate (*$P < 0.05$).

4. Discussion

Full-thickness skin defects caused by severe trauma, extensive burns and other reasons are common clinical disorders, their spontaneous healing is a dynamic and multi-stage process including inflammation, angiogenesis, matrix deposition and cell recruitment [49,50]. And there are multiple kinds of cells involved, including keratinocytes, endothelial cells, fibroblasts, inflammatory cells, etc [48]. Generally speaking, the

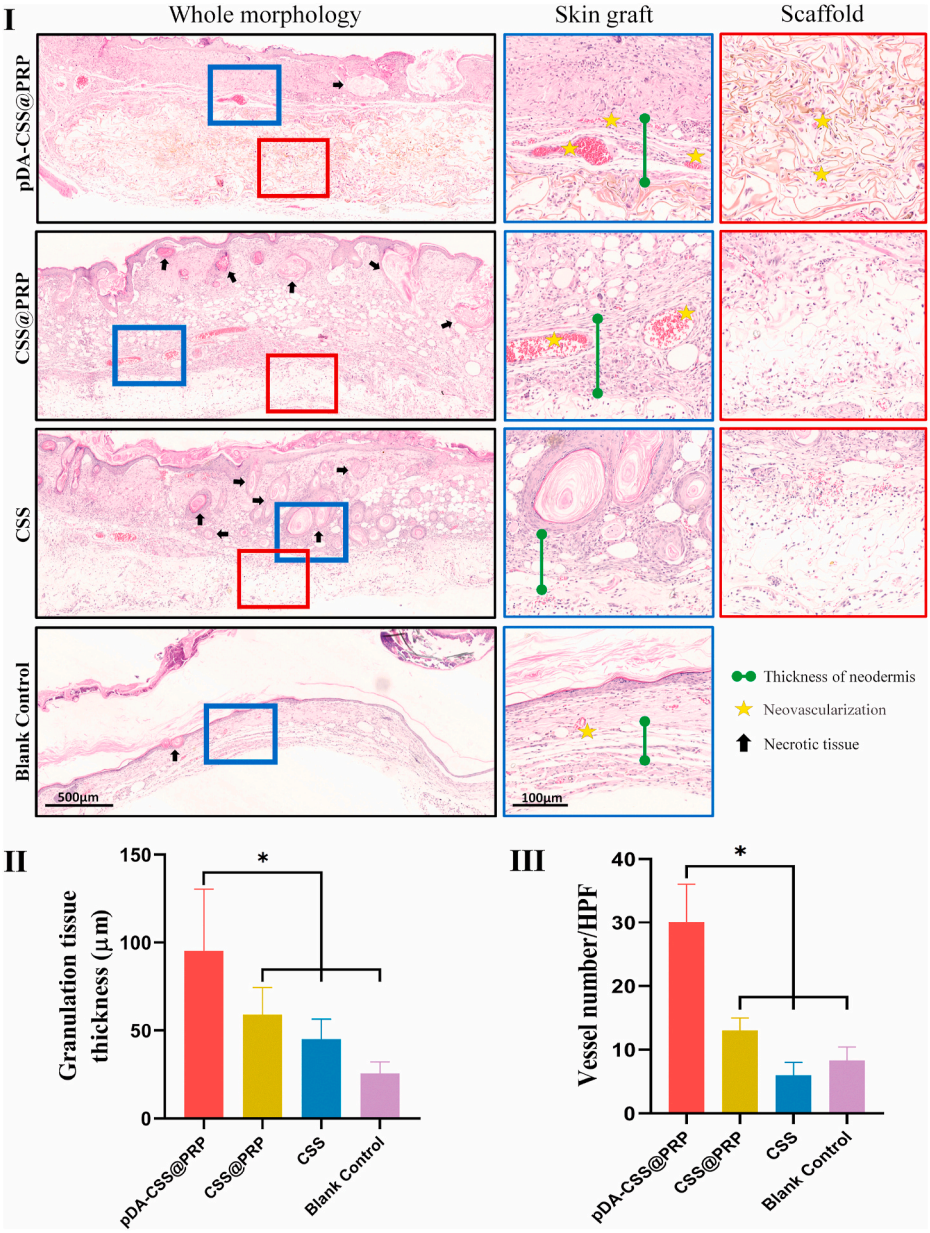

Fig. 7. Histological analysis of the skin flaps for different groups on 21st day. (I) H&E stained sections of each group. The blue solid square boxes indicate the locations investigated under higher magnification at the full-thickness skin graft layer. The red solid square boxes indicate the locations investigated under higher magnification at the scaffold layer. The high magnification images are displayed with the corresponding color frame after whole morphology. Black arrow heads indicated necrotic tissues. Yellow asterisks represent new blood vessels. The length of the green dumbbell represents the granulation tissue thickness. (II) Quantification of granulation tissue thickness. (III) Quantification of vessel number (*$P < 0.05$). (For interpretation of the references to color in this figure legend, the reader is referred to the Web version of this article.)

conventional treatment is to debride the wound and then perform skin grafting or skin flap transplantation after the wound granulation tissue grows well [2]. Compared with skin flaps transplantation, skin grafts have the distinctive advantages of less damage to the donor site and easy operation [4]. However, due to the lack of sufficient dermal matrix, skin grafts are easily hindered by uncontrollable scar hyperplasia, lower mechanical resistance, etc. in the later phase [51]. The development and application of skin tissue engineering may improve the skin graft treatment to a certain extent.

PRP has been reported to be a stocking source for various GFs (e.g., PDGF, IGF-1,VEGF, FGF-2, etc.), which stimulate neo-angiogenetic vascularization and various activities of fibroblasts [52]. VEGF is accepted as the principle stimulatory factors of angiogenesis. PDGF, capable of enlarging blood vessels and forming mature vessels, is a powerful chemoattractant for fibroblasts and smooth muscle cells. Increasing attention has been attracted for wound healing by PRP treatments, including PRP combined with mesenchymal stem cells (like adipose-derived stem cells) or stromal vascular fraction [53,54]. Based on an in-vitro and in-vivo evaluation of a bio-functionalized scaffold containing PRP and hyaluronic acid, Pietro Gentile et al. demonstrated its regenerative potential in chronic ulcers, with increased epidermal proliferation and dermal renewal [52]. Thereafter, they also reported in-vivo/in-vitro results obtained with different Kits to isolate autologous human activated or non-activated PRP, with the aim of meeting consensus quality criteria [55]. Nevertheless, application of PRP is currently limited by the short half-life period and the burst release (causing low concentration of GFs in situ) [12]. It is necessary to find solutions to improve the clinical application of PRP.

Artificial dermis is a commercially available bi-layer scaffold (including the silicone layer and the collagen-based layer), which has been widely applied in various full-thickness skin defects. The porous structure and suitable pore size of the lower layer (that is the CSS, termed as a DRT) promote cell adhesion and diffusion, and the connection of pores plays an key role in nutrient transportation and vascularization, significantly reducing contracture and scar formation [56]. Currently, the two-step surgical procedure is the universal criteria in the application of artificial dermis. Briefly, wounds are implanted with bi-layer artificial dermis following thorough wound debridement in

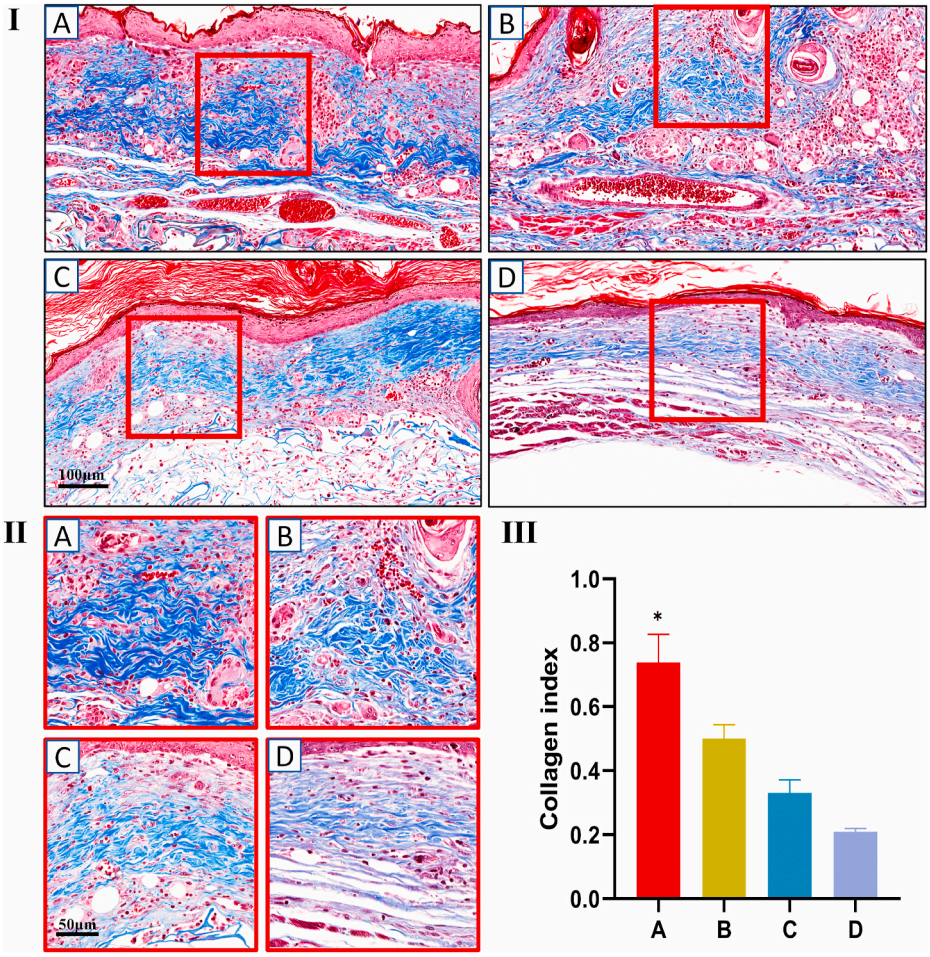

Fig. 8. Masson's trichrome stained tissue sections of all groups on days 21. (I) Collagen deposition in the skin graft sections of each group at low magnification. A, B, C and D indicate pDA-CSS@PRP, CSS@PRP, CSS and blank control, respectively. The red solid square boxes indicate the locations investigated under higher magnification. (II) Magnified view of the locations investigated for each group. (III) Statistical data of the collagen intensity of the four groups (*$P < 0.05$). (For interpretation of the references to color in this figure legend, the reader is referred to the Web version of this article.)

the first stage, and after 2–3 weeks of the DRT′ vascularization, skin grafts will be performed to cover the wound bed in the second stage [57,58]. By means of the two-step surgical procedure with bi-layer dermal substitutes, Barbara De Angelis et al. proved Nevelia® took precedence over Integra® for patients with post-traumatic injury wounds [59]. Undoubtedly, the need for two surgical procedures is not only indeed frustrating and inconvenient, but also increases the hospital stay and the risk of infection [60]. Therefore, One-step transplantation (i.e., DRT implantation and skin transplantation are performed in one surgical procedure.) implies an attractive clinical prospect, as reported by Barbara De Angelis et al. for the reconstruction of scalp after full-thickness oncologic defects with Integra® DRT [61]. However, the current DRT of artificial dermis commercially available by means of the One-step strategy will counter-intentionally form a barrier between the wound bed and the grafted skin, leading to graft failure [62]. Previous studies have suggested that PRP has positive effects on the implantation of artificial dermis. Formigli et al. [10]. reported that artificial dermis combined with PRP demonstrated an improved overall restoration of tissue functions. On the other hand, Harrison et al. [63]. explored the use of collagen as a platelet activator in PRP, proving the sustained release effect for GFs from PRP with collagen. The main challenge of this strategy is how to promote the cells' adhesion and proliferation and vascularization into the scaffolds in the short-term after surgery, thus achieving sustained and efficient tissue regeneration with enough vascularization to enable the skin grafts with desired survival.

Messersmith and coworkers [64] investigated mussel adhesion in nature and reported that dopamine, under alkaline conditions, could self-polymerize into pDA, which is rich in catechol functions. This functional groups can be converted into quinones to enhance cross-linking, providing a simple method to modify various inorganic and organic substrates [65]. With the increasing researches being performed in the past decade [66–68], pDA has been proven to possess excellent biocompatibility, adhesion and low cytotoxicity, shedding new light on the surface functionalization (e.g., photothermal performance, strong adhesive property, pH-sensitive release patterns) of various biomaterials (such as electrospinning, nanoparticles, microsphere) [30,69,70]. For instance, Zhang et al. [71]. reported that pDA can significantly reduce oxidative stress damage and improve cell viability, which promoting good cell proliferation. Zhang et al. [72]. developed a paclitaxel-loaded mesoporous silica nanoparticles which were encapsulated in pDA-coated electrospun polylactic acid fibers, with delayed early burst release of paclitaxel in-stent thrombosis, thereby avoiding the proliferation of vascular smooth muscle cells and increasing the safety of vascular stent implants. Meanwhile, the high surface charge on pDA increased the degree of oxidation of graphene oxide, which activated platelets [73].

By means of pDA modification strategy in this study, we firstly fabricated a new biomaterial based on CSS as a DRT facilitating dermis regeneration, as well as being beneficial for angiogenesis and cell chemotaxis. After being coated with a pDA layer, sterilized scaffolds were then spin-mixed in the freshly prepared PRP to make them fully loaded with platelets. As previously reported [45], the microscopic feature of artificial dermis is a porous structure with pore sizes ranging from 50 to 150 μm and a continuous radial structure, which is beneficial for more PRP adhesion, cell migration and angiogenesis. After being immersed and modified in a dopamine solution (pH = 8.5) for 12 h, some pDA nanoparticles were covalently bonded together to form a uniform pDA layer and aggregated on the CSS's surface (Fig. 1III),

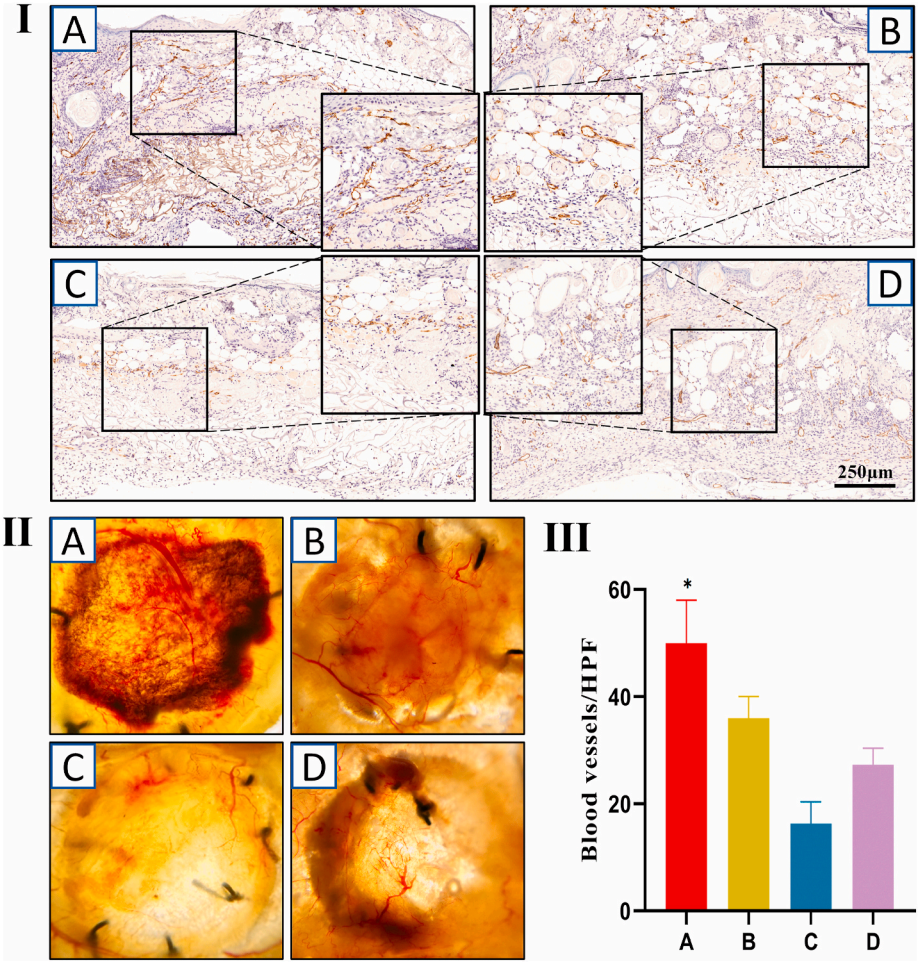

Fig. 9. Angiogenesis in vivo. (I) CD31 immunohistochemistry staining of wound sections on post operational day 14. Newly formed blood vessels were detected in the wound sites. A, B, C and D indicate pDA-CSS@PRP, CSS@PRP, CSS and blank control, respectively. (II) Gross view of wounds receiving different treatments at day 21 post-wounding from the undersurface. (III) Quantification of CD31 vessels (*$P < 0.05$).

making the pDA-CSS surface increasingly rough and dense [74,75]. Meanwhile, the microstructure via SEM demonstrated that the porous structure of CSSs didn't been destroyed. Furthermore, more platelets were immobilized on the surface of pDA-coated CSS (Fig. 2I), which indicated that pDA significantly increased the loading of PRP on CSSs, probably providing more stimulating factors for tissue formation and angiogenesis. This result above was also in accordance with the release profiles of VEGF and PDGF-BB (Fig. 2II & III). Compared with other groups, the concentration of GFs in the pDA-CSS@PRP group remained high for a long time, which means that the CSS modified by pDA loads more PRP and exerts a controlled-release effect.

Wound healing requires the extensive participation of multiple tissue cells, whose proliferation and migration are key in this process [76]. HaCaT cells (as the substitute for keratinocytes in scientific research involving re-epithelialization) [77] and HUVECs (as the substitute for endothelial cells, universally being applied to investigate angiogenesis) [78] were selected in the following in-vitro biological evaluations. As displayed in Fig. 3, the fluorescence intensity demonstrated that HaCaT cells and HUVECs well attached to the scaffolds in each group, indicating the CSS itself possess excellent properties of promoting cell adhesion, in line with the previous studies [22]. Furthermore, PRP also facilitated cell adhesion and proliferation of HaCaT cells and HUVECs, which meant its potential to promote epithelialization and vascularization. Notably, the positive effects above were further enhanced by pDA modification (Fig. 3II, $P < 0.05$), which not only indicated the excellent biocompatibility of pDA-CSS, but also further demonstrated this new scaffold capable of delivering more PRP (or platelets) created favorable conditions for cell proliferation. This was also confirmed by the scratch wound assay (Fig. 4), implying the pDA-CSS delivering PRP (or platelets) positively augmented the migration of the wound healing related cells. Prior studies have reported that collagen/PRP (COL/PRP) scaffold provides sustained release of GFs [46], which paralleled with our result. Considering these release profiles of VEGF and PDGF-BB, it is reasonable to presume that pDA-CSS might function as a novel DRT with an excellent drug delivery potential to achieve high-efficiency regeneration of full-thickness skin defects. This difference in release may also be attributed to the fact that platelets were activated through protease-activated receptor-4 (PAR-4, as the second receptor after attaching to collagen, which forms a lengthier mechanism that delays the release of GFs [79]. Of course, it was necessary to be further verified in in-vivo experiments.

In order to verify the impacts of pDA-CSS with PRP on the regeneration of in vivo wound healing, two dorsal full-thickness wound model were established on nude mice by means of the One-step strategy. To be general, full-thickness skin grafts in each group survived to some extent after being grafted, that is, unhealed wounds presented a shrinking trend with the progress of transplantation. Particularly, pDA-CSS with PRP performed significant efficacy in the survival of the skin grafts (Fig. 5). However, different from the pDA-CSS@PRP group, the skin graft and CSS are transplanted simultaneously by means of One-step strategy revealed the poorer effect of promoting wound healing due to the lack of blood supply, as prior reported, which is why the artificial dermis

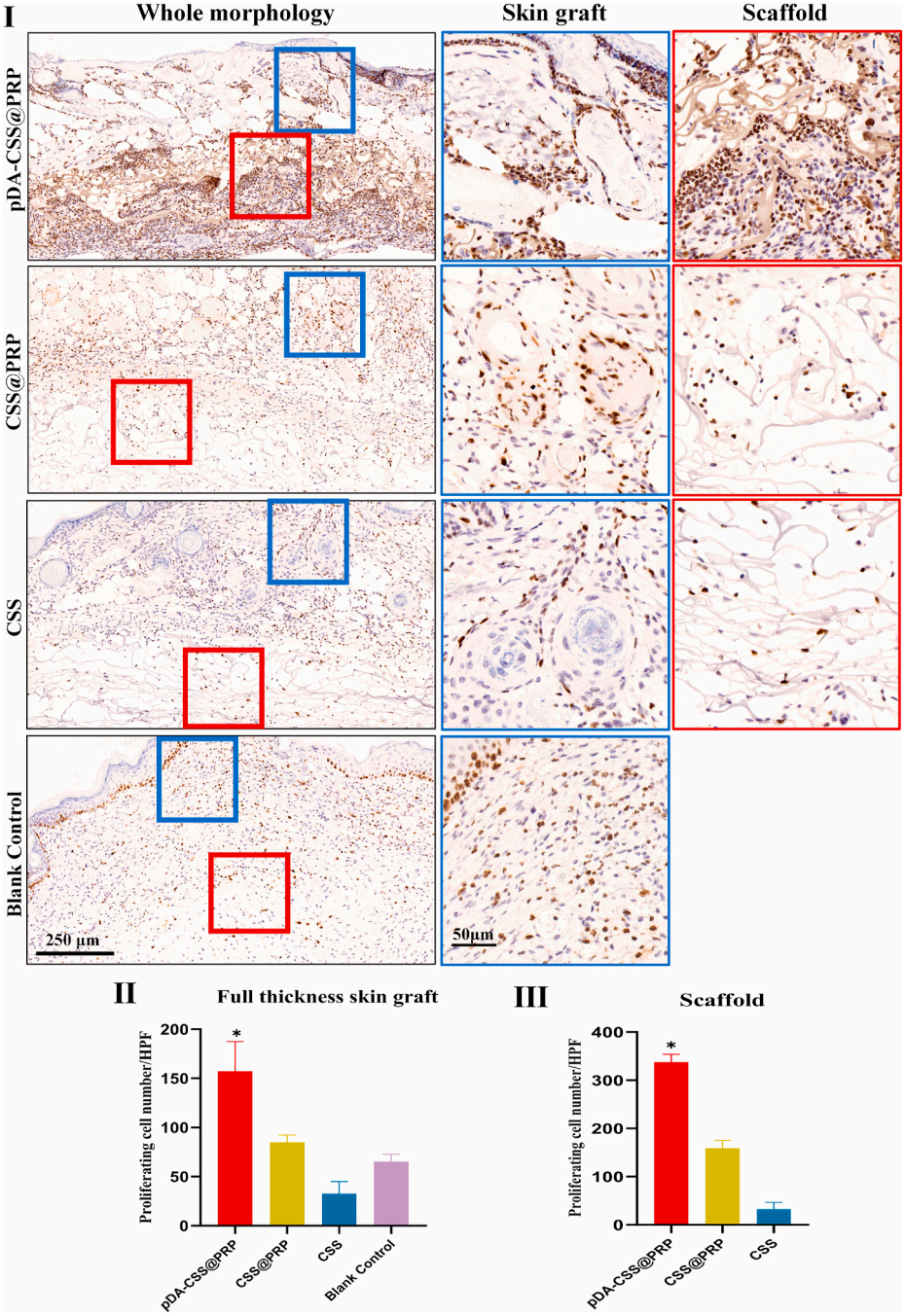

Fig. 10. Ki67 staining of proliferating cells. (I) Cell proliferation of wounds on day 14. The blue solid square boxes indicate the locations investigated under higher magnification at the full-thickness skin graft layer. The red solid square boxes indicate the locations investigated under higher magnification at the scaffold layer. The high magnification images are displayed with the corresponding color frame after whole morphology. (II) Quantification of proliferating cells number at full-thickness skin graft layer. (III) Quantification of proliferating cells number at the scaffold layer (*$P < 0.05$). (For interpretation of the references to color in this figure legend, the reader is referred to the Web version of this article.)

commercially available requires two-step skin grafting [80]. H&E and Masson trichrome staining histologically proved pDA-CSS@PRP to be capable of accelerating the healing process (Figs. 7 and 8), which was mainly reflected in the fact that pDA-CSS@PRP promoted the formation of prolific granulation tissue and the predetermined arrangement of more mature collagen. Totally, it is reasonably inferred that pDA-CSS@PRP's positive effects on wound repair may be according to the following aspects: Firstly, the porous and well-biocompatible CSS, as the basic scaffold of a DRT, essentially facilitates the ideal colonization of skin repair related cells (e.g., fibroblasts, HUVECs, keratinocytes, etc.) with enhanced biological activities. And the porous structure tends to be infiltrated and filled by extracellular matrix, including fibrin, pro-collagen molecules, lysyl oxidase, etc [81]. By the way, lysyl oxidase and collagen can be further cross-linked to achieve long-term strength and stability [82]. Secondly, it is universally acknowledged that the repair and regeneration of tissues require multiple GFs' cooperative participation [83]. Unlike the clinical practice just using one or two GFs, the promising PRP in this study comprehensively provided more GFs for wound healing, of which VEGF and PDGF-BB are especially important in cell proliferation and angiogenesis [84,85]. Thirdly, as an important interface modifier, pDA not only improved biocompatibility [30], but also furtherly inspired the surface immobilization of bioactive molecules. On the one hand, the activated surface can facilitate the recruitment of more repair related cells (e.g., fibroblasts, vascular endothelial cells, inflammatory cells, etc.) and induce them to colonize in situ. On the other hand, the enhanced adhesion property improves the loading capacity and controlled release effect of these scaffolds delivering PRP (or platelets), maintaining the concentration of local GFs at a high level. In this case, angiogenesis and tissue repair will be achieved more efficiently, which provides desired conditions for the survival rate of

full-thickness skin graft, as well as the healing and regeneration of skin wounds.

There are still some issues deserving attention. In this study, pigs were used to obtain enough blood to uniformly prepare PRP in large amounts. And in order to better mimic the autologous application of PRP in clinical practice [52], non-immunogenic nude mice were applied to construct full-thickness skin defects. Since the end point of animal experiment was day 21, the degradation characteristics of pDA-CSS@PRP in vivo haven't been collected for the time being, which will be improved in our researches in the near future. In addition, considering that there were two different groups on the back of each mouse (following the principle of homologous control [86]), we failed to compare the differences in the in-vivo release of GFs in each group by collecting mouse whole blood. Furthermore, unlike STSGs clinically recommended as skin grafts [87], full-thickness skin grafts were applied in this experiment in order to reduce system errors (caused by inconsistent and difficult surgical operations of skin removal on such petite nude mice). And interestingly, full-thickness skin grafts displayed expected survival in this experiment, although it is theoretically not as easy to survive as STSG. Logically, doesn't it mean that the results of this study may provide more references for the applicability of STSG? Notably, no significant difference was observed among the four groups regarding their wound shrinkage rate, which might be attributed to the end time point or types of skin grafts (Fig. 6). A more comprehensive research with long-term effect observation and standardized STSG (as clinical practice) should be focused on and performed in future.

5. Conclusions

In summary, we successfully constructed a composite of pDA and CSS, which can load more PRP to increase the release and duration of GFs for the treatment of full-thickness skin defects. Both in vivo and in vitro, the complexes maintained the biological activity of PRP and promoted angiogenesis and cell proliferation. This study demonstrates that pDA modified CSS can load more PRP to stimulate early angiogenesis in full-thickness skin defects and promote wound healing and skin remodeling, which provides more options for the design of biological tissue engineering materials.

CRediT authorship contribution statement

Zijun Zheng: Investigation, Writing - original draft. **Minxiong Li:** Methodology, Writing - review & editing. **Pengewei Shi:** Validation, Formal analysis. **Yanbin Gao:** Data curation, Validation. **Jun Ma:** Project administration, Writing - review & editing. **Yuchen Li & Lei Huang:** Validation, Writing - revision recheck. Zhangfeifan Yang: Statistical validation**Lei Yang:** Conceptualization, Project administration, Funding acquisition.

Declaration of competing interest

The authors declare no conflict of interest.

Acknowledgements

This work was supported by the Natural Science Foundation of Guangdong Province [No.2020A151501108], the Guangdong Province Key Field R&D Program Project [No. 2020B1111150001], the Science and Technology Innovation Project of Guangdong Province [No. 2018KJYZ005], the Natural Science Foundation of Tibet Autonomous Region [No. XZ2017ZR-ZY021].

Abbreviations

3D	three-dimensional
AFM	atomic force microscope
BSA	bovine serum albumin
COL/PRP	collagen/PRP
CSS(s)	collagen sponge scaffold(s)
DA	dopamine
DAPI	4′, 6-diamidino-2-phenylindole
DRT	dermal regenerate template
ELISA	enzyme-linked immunosorbent assay
FGF-2	fibroblast growth factor-2
GF(s)	growth factor(s)
H&E	Hematoxylin and Eosin
HaCaT cells	human immortalized keratinocytes
HPF	high power field
HUVEC(s)	human umbilical vein endothelial cell(s)
IACUC	institutional animal care and use committee
IGF-1	insulin-like growth factors-1
LSCM	laser scanning confocal microscopy
MR	migration rate
NS	normal saline
PBS	phosphate buffered saline
pDA	polydopamine
PDGF-BB	platelet-derived growth factor-BB
PPP	platelet-poor plasma
PRP	platelets-rich plasma
SEM	scanning electron microscope
STSG(s)	split thickness skin graft(s)
TGF-β:	transforming growth factor-β
VEGF	vascular endothelial growth factor

References

[1] E.S. Chambers, M. Vukmanovic-Stejic, Skin barrier immunity and ageing, Immunology 160 (2) (2020) 116–125.
[2] E.A. Lucich, J.L. Rendon, I.L. Valerio, Advances in addressing full-thickness skin defects: a review of dermal and epidermal substitutes, Regen. Med. 13 (4) (2018) 443–456.
[3] M.B. Dreifke, A.A. Jayasuriya, A.C. Jayasuriya, Current wound healing procedures and potential care, Mater Sci Eng C Mater Biol Appl 48 (2015) 651–662.
[4] R. Shimizu, K. Kishi, Skin graft, Plast Surg Int (2012) 563493, 2012.
[5] J.H. Zhao, et al., Clinical application of full-face, whole, full-thickness skin grafting: a case report, J. Plast. Reconstr. Aesthetic Surg. 65 (11) (2012) 1576–1579.
[6] J. Yang, et al., Umbilical cord-derived mesenchymal stem cell-derived exosomes combined pluronic F127 hydrogel promote chronic diabetic wound healing and complete skin regeneration, Int. J. Nanomed. 15 (2020) 5911–5926.
[7] P. Everts, et al., Platelet-rich plasma: new performance understandings and therapeutic considerations in 2020, Int. J. Mol. Sci. 21 (20) (2020).
[8] M.J. Hesseler, N. Shyam, Platelet-rich plasma and its utility in the treatment of acne scars: a systematic review, J. Am. Acad. Dermatol. 80 (6) (2019) 1730–1745.
[9] D. Steller, et al., Impact of incubation method on the release of growth factors in non-Ca(2+)-activated PRP, Ca(2+)-activated PRP, PRF and A-PRF, J. Cranio-Maxillo-Fac. Surg. 47 (2) (2019) 365–372.
[10] L. Formigli, et al., Dermal matrix scaffold engineered with adult mesenchymal stem cells and platelet-rich plasma as a potential tool for tissue repair and regeneration, J Tissue Eng Regen Med 6 (2) (2012) 125–134.
[11] Q. Chang, et al., Large adipose tissue generation in a mussel-inspired bioreactor of elastic-mimetic cryogel and platelets, J. Tissue Eng. 9 (2018), 2041731418808633.
[12] X. Liu, et al., An in situ photocrosslinkable platelet rich plasma - complexed hydrogel glue with growth factor controlled release ability to promote cartilage defect repair, Acta Biomater. 62 (2017) 179–187.
[13] G. Ho, et al., A systematic review and meta-analysis of complications associated with acellular dermal matrix-assisted breast reconstruction, Ann. Plast. Surg. 68 (4) (2012) 346–356.
[14] J.L. Wester, et al., AlloDerm with split-thickness skin graft for coverage of the forearm free flap donor site, Otolaryngol. Head Neck Surg. 150 (1) (2014) 47–52.
[15] M.S. Fourman, et al., Laser-assisted indocyanine green dye angiography accurately predicts the split-thickness graft timing of integra artificial dermis, Ann. Plast. Surg. 73 (2) (2014) 150–155.
[16] L.E.M. de Haas, et al., The use of integra in extensive full-thickness scalp burn involving the skull in a child, J. Craniofac. Surg. 30 (3) (2019) 888–890.
[17] S.C. Notodihardjo, et al., A comparison of the wound healing process after the application of three dermal substitutes with or without basic fibroblast growth factor impregnation in diabetic mice, J. Plast. Reconstr. Aesthetic Surg. 73 (8) (2020) 1547–1555.
[18] T. Su, et al., Mussel-inspired agarose hydrogel scaffolds for skin tissue engineering, Bioact Mater 6 (3) (2021) 579–588.

[19] J. Hou, et al., Sustained release of N-acetylcysteine by sandwich structured polycaprolactone/collagen scaffolds for wound healing, J. Biomed. Mater. Res. 107 (7) (2019) 1414–1424.
[20] Y. Chen, et al., Targeted pathological collagen delivery of sustained-release rapamycin to prevent heterotopic ossification, Sci Adv 6 (18) (2020), eaay9526.
[21] Y.Z. Wang, et al., Biomimetic fibroblast-loaded artificial dermis with "sandwich" structure and designed gradient pore sizes promotes wound healing by favoring granulation tissue formation and wound re-epithelialization, Acta Biomater. 30 (2016) 246–257.
[22] M. Li, et al., Epithelial differentiation of human adipose-derived stem cells (hASCs) undergoing three-dimensional (3D) cultivation with collagen sponge scaffold (CSS) via an indirect co-culture strategy, Stem Cell Res. Ther. 11 (1) (2020) 141.
[23] S.R. Jackson, S. Roman, Matriderm and split skin grafting for full-thickness pediatric facial burns, J. Burn Care Res. 40 (2) (2019) 251–254.
[24] T. Liu, et al., One-step approach for full-thickness skin defect reconstruction in rats using minced split-thickness skin grafts with Pelnac overlay, Burns Trauma 7 (2019) 19.
[25] R.R. Costa, J.F. Mano, Polyelectrolyte multilayered assemblies in biomedical technologies, Chem. Soc. Rev. 43 (10) (2014) 3453–3479.
[26] M. Mehdizadeh, et al., Injectable citrate-based mussel-inspired tissue bioadhesives with high wet strength for sutureless wound closure, Biomaterials 33 (32) (2012) 7972–7983.
[27] M. Liang, et al., A high-strength double network polydopamine nanocomposite hydrogel for adhesion under seawater, J. Mater. Chem. B 8 (36) (2020) 8232–8241.
[28] R. Batul, et al., Recent progress in the biomedical applications of polydopamine nanostructures, Biomater Sci 5 (7) (2017) 1204–1229.
[29] K.S. Shalini Devi, S. Jacob, A. Senthil Kumar, In situ structural Elucidation and selective Pb(2+) ion recognition of polydopamine film formed by controlled electrochemical oxidation of dopamine, Langmuir 34 (24) (2018) 7048–7058.
[30] H.Q. Tran, et al., Current advances in the utilization of polydopamine nanostructures in biomedical therapy, Biotechnol. J. 14 (12) (2019), e1900080.
[31] V. Ball, et al., Kinetics of polydopamine film deposition as a function of pH and dopamine concentration: insights in the polydopamine deposition mechanism, J. Colloid Interface Sci. 386 (1) (2012) 366–372.
[32] X. Liu, et al., Mussel-inspired polydopamine: a biocompatible and ultrastable coating for nanoparticles in vivo, ACS Nano 7 (10) (2013) 9384–9395.
[33] T. Chen, et al., Biodegradable 3D printed HA/CMCS/PDA scaffold for repairing lacunar bone defect, Mater Sci Eng C Mater Biol Appl 116 (2020) 111148.
[34] Q. Lu, et al., SO2 prodrug doped nanorattles with extra-high drug payload for "collusion inside and outside" photothermal/pH triggered - gas therapy, Biomaterials 257 (2020) 120236.
[35] Y. Zhang, et al., Smart oral administration of polydopamine-coated nanodrugs for efficient attenuation of radiation-induced gastrointestinal syndrome, Adv Healthc Mater 9 (13) (2020), e1901778.
[36] M. Razavi, et al., Controlled nutrient delivery to pancreatic islets using polydopamine-coated mesoporous silica nanoparticles, Nano Lett. 20 (10) (2020) 7220–7229.
[37] B. Zhang, et al., Construction of tendon replacement tissue based on collagen sponge and mesenchymal stem cells by coupled mechano-chemical induction and evaluation of its tendon repair abilities, Acta Biomater. 74 (2018) 247–259.
[38] K.T.L. Trinh, N.X.T. Le, N.Y. Lee, Chitosan-polydopamine hydrogel complex: a novel green adhesion agent for reversibly bonding thermoplastic microdevice and its application for cell-friendly microfluidic 3D cell culture, Lab Chip 20 (19) (2020) 3524–3534.
[39] Y. Liang, et al., Application of stable continuous external electric field promotes wound healing in pig wound model, Bioelectrochemistry 135 (2020) 107578.
[40] G. Qiu, et al., Bone regeneration in minipigs via calcium phosphate cement scaffold delivering autologous bone marrow mesenchymal stem cells and platelet-rich plasma, J Tissue Eng Regen Med 12 (2) (2018) e937–e948.
[41] S.P. Mohan, et al., Platelet-rich plasma and platelet-rich fibrin in periodontal regeneration: a review, J. Pharm. BioAllied Sci. 11 (Suppl 2) (2019) S126–S130.
[42] F. Zhou, et al., Prevascularized mesenchymal stem cell-sheets increase survival of random skin flaps in a nude mouse model, Am J Transl Res 11 (3) (2019) 1403–1416.
[43] F. Prattichizzo, et al., CD31 positive-extracellular vesicles from patients with type 2 diabetes shuttle a miRNA signature associated with cardiovascular complications, Diabetes 70 (1) (2020) 240–254.
[44] X. Li, et al., Single-cell RNA-seq reveals that CD9 is a negative marker of glucose-responsive pancreatic beta-like cells derived from human Pluripotent stem cells, Stem Cell Reports 15 (5) (2020) 1111–1126.
[45] H. Wang, et al., Mussel-inspired polydopamine coating: a general strategy to enhance osteogenic differentiation and osseointegration for diverse implants, ACS Appl. Mater. Interfaces 11 (7) (2019) 7615–7625.
[46] X. Zhang, et al., A novel collagen/platelet-rich plasma (COL/PRP) scaffold: preparation and growth factor release analysis, Cell Tissue Bank. 17 (2) (2016) 327–334.
[47] G.H. Zhang, et al., Angiotensin II enhances the proliferation of Natural Killer/T-cell lymphoma cells via activating PI3K/Akt signaling pathway, Biosci. Rep. 40 (10) (2020).
[48] L. Chen, et al., Pre-vascularization enhances therapeutic effects of human mesenchymal stem cell sheets in full thickness skin wound repair, Theranostics 7 (1) (2017) 117–131.
[49] S.H. Moreira, et al., Evaluation of angiogenesis, inflammation, and healing on irradiated skin graft with low-level laser therapy in rats (Rattus norvegicus albinus wistar), Laser Med. Sci. 35 (5) (2020) 1103–1109.
[50] N. Alexandrushkina, et al., Cell sheets from adipose tissue MSC induce healing of pressure ulcer and prevent fibrosis via trigger effects on granulation tissue growth and vascularization, Int. J. Mol. Sci. 21 (15) (2020).
[51] S.A. Eming, P. Martin, M. Tomic-Canic, Wound repair and regeneration: mechanisms, signaling, and translation, Sci. Transl. Med. 6 (265) (2014) 265sr6.
[52] B. De Angelis, et al., Wound healing: in vitro and in vivo evaluation of a bio-functionalized scaffold based on hyaluronic acid and platelet-rich plasma in chronic ulcers, J. Clin. Med. 8 (9) (2019).
[53] P. Gentile, et al., Concise review: the use of adipose-derived stromal vascular fraction cells and platelet rich plasma in regenerative plastic surgery, Stem Cell. 35 (1) (2017) 117–134.
[54] V. Cervelli, et al., Application of enhanced stromal vascular fraction and fat grafting mixed with PRP in post-traumatic lower extremity ulcers, Stem Cell Res. 6 (2) (2011) 103–111.
[55] P. Gentile, et al., Impact of the different preparation methods to obtain autologous non-activated platelet-rich plasma (A-PRP) and activated platelet-rich plasma (AA-PRP) in plastic surgery: wound healing and hair regrowth evaluation, Int. J. Mol. Sci. 21 (2) (2020).
[56] L. Ma, C. Gao, J. Shen, [Factors controlling the microstructure of collagen-based dermis regeneration scaffold], Sheng Wu Yi Xue Gong Cheng Xue Za Zhi 21 (2) (2004) 311–315.
[57] X. Qiu, et al., Vascularization of Lando((R)) dermal scaffold in an acute full-thickness skin-defect porcine model, J Plast Surg Hand Surg 52 (4) (2018) 204–209.
[58] V. Watts, M.D. Attie, S. McClure, Reconstruction of complex full-thickness scalp defects after dog-bite injuries using dermal regeneration template (integra): case report and literature review, J. Oral Maxillofac. Surg. 77 (2) (2019) 338–351.
[59] B. De Angelis, et al., Long-term follow-up comparison of two different bi-layer dermal substitutes in tissue regeneration: clinical outcomes and histological findings, Int. Wound J. 15 (5) (2018) 695–706.
[60] M. Demircan, T. Cicek, M.I. Yetis, Preliminary results in single-step wound closure procedure of full-thickness facial burns in children by using the collagen-elastin matrix and review of pediatric facial burns, Burns 41 (6) (2015) 1268–1274.
[61] B. De Angelis, et al., One-stage reconstruction of scalp after full-thickness oncologic defects using a dermal regeneration template (integra), BioMed Res. Int. 2015 (2015) 698385.
[62] D. Heimbach, et al., Artificial dermis for major burns. A multi-center randomized clinical trial, Ann. Surg. 208 (3) (1988) 313–320.
[63] S. Harrison, et al., Platelet activation by collagen provides sustained release of anabolic cytokines, Am. J. Sports Med. 39 (4) (2011) 729–734.
[64] H. Lee, et al., Mussel-inspired surface chemistry for multifunctional coatings, Science 318 (5849) (2007) 426–430.
[65] S. Liu, et al., Polydopamine-coated chitosan/calcium pyrophosphate hybrid microflowers as an effective hemostatic agent, Carbohydr. Polym. 224 (2019) 115175.
[66] P. Jiang, A. Choi, K.E. Swindle-Reilly, Controlled release of anti-VEGF by redox-responsive polydopamine nanoparticles, Nanoscale 12 (33) (2020) 17298–17311.
[67] M. Godoy-Gallardo, et al., Immobilization of BMP-2 and VEGF within multilayered polydopamine-coated scaffolds and the resulting osteogenic and angiogenic synergy of Co-cultured human mesenchymal stem cells and human endothelial progenitor cells, Int. J. Mol. Sci. 21 (17) (2020).
[68] S. Luo, et al., An injectable, bifunctional hydrogel with photothermal effects for tumor therapy and bone regeneration, Macromol. Biosci. 19 (9) (2019), e1900047.
[69] S. Hong, et al., Attenuation of the in vivo toxicity of biomaterials by polydopamine surface modification, Nanomedicine (Lond) 6 (5) (2011) 793–801.
[70] Y. Shan, et al., Polydopamine-modified metal-organic frameworks, NH2-Fe-MIL-101, as pH-sensitive nanocarriers for controlled pesticide release, Nanomaterials 10 (10) (2020).
[71] S. Zhang, et al., Polydopamine/puerarin nanoparticle-incorporated hybrid hydrogels for enhanced wound healing, Biomater Sci 7 (10) (2019) 4230–4236.
[72] Y. Zhang, et al., An electrospun fiber-covered stent with programmable dual drug release for endothelialization acceleration and lumen stenosis prevention, Acta Biomater. 94 (2019) 295–305.
[73] G. Li, et al., Polydopamine reinforced hemostasis of a graphene oxide sponge via enhanced platelet stimulation, Colloids Surf. B Biointerfaces 174 (2019) 35–41.
[74] J. Jiang, et al., Surface characteristics of a self-polymerized dopamine coating deposited on hydrophobic polymer films, Langmuir 27 (23) (2011) 14180–14187.
[75] D. Zheng, et al., Synthesis and characterization of dopamine-modified Ca-alginate/poly(N-isopropylacrylamide) microspheres for water retention and multi-responsive controlled release of agrochemicals, Int. J. Biol. Macromol. 160 (2020) 518–530.
[76] M. Ono, et al., CCN4/WISP1 controls cutaneous wound healing by modulating proliferation, migration and ECM expression in dermal fibroblasts via alpha5beta1 and TNFalpha, Matrix Biol. 68–69 (2018) 533–546.
[77] Y. Zhao, et al., USP15 enhances Re-epithelialization through deubiquitinating EIF4A1 during cutaneous wound repair, Front Cell Dev Biol 8 (2020) 529.
[78] S. Ren, et al., Microvesicles from human adipose stem cells promote wound healing by optimizing cellular functions via AKT and ERK signaling pathways, Stem Cell Res. Ther. 10 (1) (2019) 47.
[79] L. Jiang, et al., A critical role of thrombin/PAR-1 in ADP-induced platelet secretion and the second wave of aggregation, J. Thromb. Haemostasis 11 (5) (2013) 930–940.
[80] N. Scuderi, et al., The use of dermal regeneration template (Pelnac(R)) in a complex upper limb trauma: the first Italian case report, Eur. Rev. Med. Pharmacol. Sci. 23 (13) (2019) 5531–5534.

[81] N. Bock, et al., Polydopamine coating of uncrosslinked chitosan as an acellular scaffold for full thickness skin grafts, Carbohydr. Polym. 245 (2020) 116524.
[82] S.D. Vallet, S. Ricard-Blum, Lysyl oxidases: from enzyme activity to extracellular matrix cross-links, Essays Biochem. 63 (3) (2019) 349–364.
[83] I.H. Bae, J.W. Park, D.Y. Kim, Enhanced regenerative healing efficacy of a highly skin-permeable growth factor nanocomplex in a full-thickness excisional mouse wound model, Int. J. Nanomed. 9 (2014) 4551–4567.
[84] B.M. Borena, et al., Regenerative skin wound healing in mammals: state-of-the-art on growth factor and stem cell based treatments, Cell. Physiol. Biochem. 36 (1) (2015) 1–23.
[85] P. Wang, et al., In situ formed anti-inflammatory hydrogel loading plasmid DNA encoding VEGF for burn wound healing, Acta Biomater. 100 (2019) 191–201.
[86] C.O. Chantre, et al., Production-scale fibronectin nanofibers promote wound closure and tissue repair in a dermal mouse model, Biomaterials 166 (2018) 96–108.
[87] E. Querol-Cisneros, P. Redondo, Split-thickness skin graft strips obtained with DermaBlade to cover large surgical defects on scalp, J. Am. Acad. Dermatol. 78 (6) (2018) e145–e147.